Bioferroelectric Properties of Glycine Crystals

Pengfei Hu,[†,‡] Shunbo Hu,[‡,#] Yundi Huang,[†,‡] Jeffrey R. Reimers,[‡,§] Andrew M. Rappe,[∥] Yongle Li,*[,‡] Alessandro Stroppa,*[,⊥] and Wei Ren*[,‡,#]

[†]Department of Chemistry, Shanghai University, Shanghai 200444, China

[‡]Department of Physics, International Center of Quantum and Molecular Structures and Shanghai Key Laboratory of High Temperature Superconductors, Shanghai University, Shanghai 200444, China

[§]School of Mathematical and Physical Sciences, University of Technology, Sydney, New South Wales 2007, Australia

[∥]Department of Chemistry, University of Pennsylvania, Philadelphia, Pennsylvania 19104-6323, United States

[⊥]CNR-SPIN, c/o Dip.to di Scienze Fisiche e Chimiche - Via Vetoio - 67100 - Coppito (AQ), Italy

[#]Materials Genome Institute, Shanghai University, Shanghai 200444, China

S *Supporting Information*

ABSTRACT: Biological ferroelectric materials have great potential in biosensing and disease diagnosis and treatment. Glycine crystals form the simplest bioferroelectric materials, and here we investigate the polarizations of its β- and γ-phases. Using density functional theory, we predict that glycine crystals can develop polarizations even larger than those of conventional inorganic ferroelectrics. Further, using systematic molecular dynamics simulations utilizing polarized crystal charges, we predict the Curie temperature of γ-glycine to be 630 K, with a required coercive field to switch its polarization states of 1 V·nm^{-1}, consistent with experimental evidence. This work sheds light on the microscopic mechanism of electric dipole ordering in biomaterials, helping in the material design of novel bioferroelectrics.
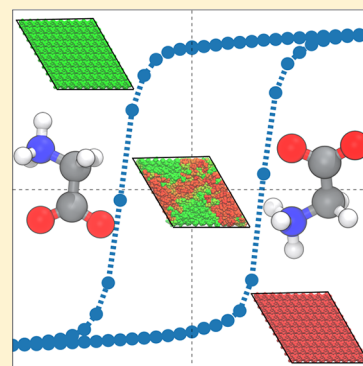
The study of ferroelectricity and piezoelectricity in biosystems provides an exciting combination of physics and biology,[1] inaugurated by the discovery of piezoelectric properties in wood by Fukada in the 1950s.[2] With modern advanced experimental techniques, piezoelectric and ferroelectric properties of many other biomaterials have been recently discovered, including properties of bones, aortic walls, nails, teeth, seashells, and peptide nanotubes.[3−9] However, little is known concerning the general principles depicting ferroelectric switching, owing to the complexity of biological materials.[10] An example comes from the recent study of Hu et al. that discussed switchable dipole long-range ordering in an important biomaterial, hydroxyapatite, using first-principles calculations.[11]

Recently, it was demonstrated that a basic component of biological structure, namely glycine, presents nanoscale ferroelectricity,[12] with an exhibited technologically significant piezoelectric response; the predicted longitudinal strain coefficient of γ-glycine, d_{33}, is about 10.4 pm V^{-1}, and the longitudinal piezoelectric coefficient, d_{22}, of β-glycine is about −5.7 pm V^{-1}.[13] Our study confirm those results, with d_{33} = 8.1 pm V^{-1} and d_{22} = −4.7 pm V^{-1}. Glycine is one of the simplest and smallest biological molecules. It therefore presents a starting point for the design of functional materials as it can be synthetically modified to optimize properties. As it is a basic building block of life,[14] it also represents a paradigm for the understanding of bioferroelectricity. Much is known about its crystal phases,[15] but very little is known about the mechanism of its ferroelectric transitions.

Glycine crystal mostly occurs in α-, β-, or γ-phases under ambient conditions.[16] Alternative δ-, ε-, and ζ-phases are known but metastable, being observable only under special conditions.[17,18] α-Glycine (symmetry group $P2_1/m$) has an antiparallel layered hydrogen bond (HB) network,[16] making it stable at room temperature. Similarly, β-glycine (symmetry group $P2_1$)[19] is also stabilized by a parallel layered HB network. Under ambient conditions, β-glycine usually transforms spontaneously into either α- or γ-phases. Among all the phases, γ-glycine is the most stable.[20] It has a helical HB network, a feature not found in the other two main phases. These three dominant phases have relative stability $\gamma > \alpha > \beta$. Another feature of technological relevance is that phases can interconvert under certain conditions, including in response to humidity changes,[21] with only the γ-phase remaining unconditionally stable in moist air;[15] phase transition from β-glycine to either α- or γ-glycine occurs when the humidity increases. Similarly, the α-phase can also change to the γ-phase under high humidity. When the temperature increases above 443 K,
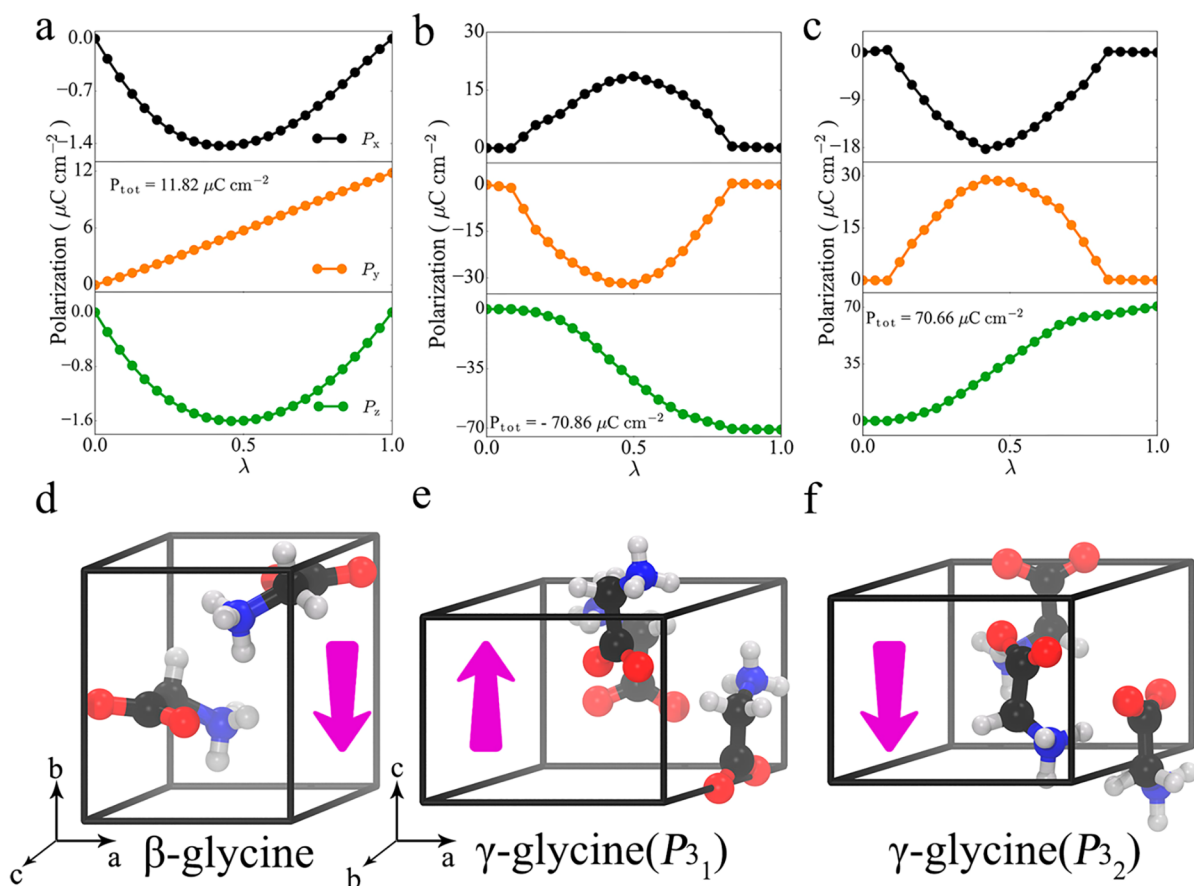
Figure 1. MPT variation of the polarization of (a) β-glycine, (b) γ-glycine ($P3_1$), and (c) γ-glycine ($P3_2$), along the path between the hypothetical paraelectric ($\lambda = 0$) and observed ferroelectric ($\lambda = 1$) phases. (d−f) Corresponding structures of glycine crystals. Color code: black, carbon; red, oxygen; blue, nitrogen; white, hydrogen. The purple arrows represents the net polarization.

the γ-phase can change to the α-phase.[21,22] Because $P2_1/m$ is centrosymmetric, there is no net polarization within the α-phase, while the polar phases, β- and γ-, have polarization along the b-axis and c-axis, respectively. The polymorphism observed among the three major phases of glycine is summarized in Figure S1 in the Supporting Information.

Glycine crystals have been previously simulated,[23] but a deep study of the potential bio-ferroelectric properties was not addressed. In this Letter, we perform first-principles density functional theory (DFT) calculations and molecular dynamics (MD) simulations, elucidating the ferroelectric properties of glycine, including both the equilibrium polarizations and the dynamic phase transition mechanism. In particular, we consider the β- (monoclinic, $P2_1$) and γ- (triangular, $P3_1$ and $P3_2$) phases using modern polarization theory (MPT), and more calculation details are in the Supporting Information.[24−26] Furthermore, we employ MD simulations with a polarized force field to study polarization switching of γ-phase. We simulate the hysteresis loop and the γ-phase transition as a function of the temperature, reproducing the reduction of the polarization that occurs as the paraelectric phase is approached.

The exchange−correlation functional used throughout the work is Perdew−Burke−Ernzerhof (PBE),[27] chosen after benchmark calculations. Detailed results and the electronic structures of glycine crystals are given in the Supporting Information (see Figures S2−S5 and Table S1).

As described in Methods in the Supporting Information, application of MPT requires the construction of a transition pathway from the observed ferroelectric phases to suitable proposed paraelectric reference structures. These pathways are divided into two parts: a pure atomic translation, i.e., a displacement−distortion field, and a coherent rotation of the molecules, i.e., a rotational distortion field. In the calculations, the paths from the reference structure to the ferroelectric structure are obtained by evenly interpolating, but they do not represent real low-energy switching paths; their purpose is simply to calculate the polarization unambiguously.[11]

The total polarization calculated for β-glycine is calculated to be 11.8 $\mu C \cdot cm^{-2}$ along the b-axis, with the components along the other two axes canceling out because of symmetry. The smooth curve shown in Figure 1a indicates that the calculation is not affected by polarization quanta.[11] In particular, we find that the ferroelectricity of β-glycine stems from an ordered arrangement of the $-NH_3^+$ group, giving rise to a weak-ferroelectric arrangement[28] and resulting in an accumulated component of dipole moment along the b-axis, and the change of improper dihedral angle between the N atom on the $-NH_3^+$ group and the plane formed by the carboxyl acid group ($-COO^-$) affects the magnitude of the resulting polarization. For polarization along the b-axis, the $-NH_3^+$ group undergoes a transition from the paraelectric structure to the ferroelectric one.

On the other hand, the polarization of γ-glycine is extraordinarily large, reaching 70.9 $\mu C \cdot cm^{-2}$ along the c-axis

for the $P3_1$ phase and 70.7 $\mu C \cdot cm^{-2}$ for the $P3_2$ phase. Along the transition path, the glycine molecules rotate by 180° around an axis perpendicular to the c-axis. Polarizations for the two γ-glycine phases (Figure 1b,c) are about five times larger than that for β-glycine (Figure 1a) and are similar to those for traditional ferroelectric materials.[29−31] Glycine is a polar molecule with a large molecular dipole moment of 11.5 D.[23] Although the molecular volumes in the crystals are similar for both β- and γ-glycine, in β-glycine different molecules have their dipoles in different directions, whereas in γ-glycine the moments are helically aligned, with a net component along the c-axis (Figure 1).

To gain more insight into the origin of ferroelectricity in glycine, systematic MD simulations were performed using the polarized crystal charge (PCC) based on the protein-specific polarized charge (PPC),[32,33] examining the response of the crystal structure and its polarization to an applied external electric field at 300 K. Here we considered only the γ-phase (symmetry group $P3_2$) because the β-phase is extremely unstable and unlikely to be utilized in any application. During the simulation, an external electric field was applied along the c-axis. Its magnitude varies from 0 to 3 $V \cdot nm^{-1}$, then to −3 $V \cdot nm^{-1}$, and then returns to zero. Results are shown in Figure 2.
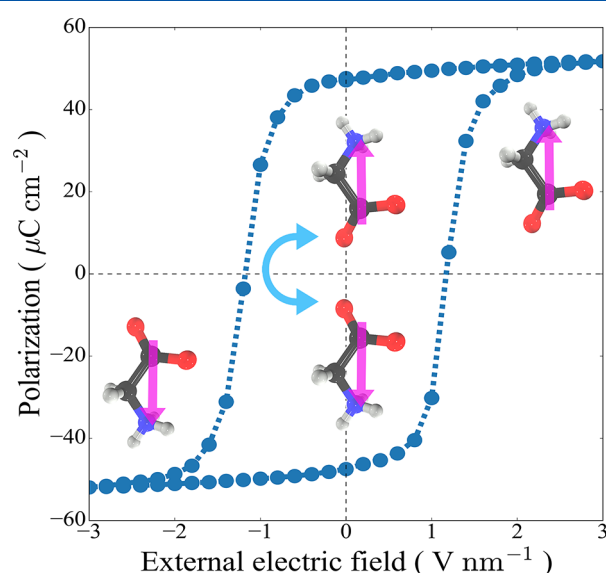

Figure 2. Hysteresis loop from MD shows polarization switching of γ-glycine as controlled by an external applied electric field at 300 K.

Increasing the magnitude of the applied field |E| induced a switching from one fully aligned ferroelectric molecular arrangement to the other. This switching occurred throughout the range 1 $V \cdot nm^{-1}$ < |E| < 2 $V \cdot nm^{-1}$, creating a hysteresis loop. Although the magnitude of the field required to induce switching is quite large, it is not outside the experimentally accessible range in both Stark experiments and in electrical devices. Also, the Landauer paradox[34] will apply to this result, indicating that simulations of realistic multicrystalline materials will be predicted to have smaller switching fields than that perceived in the current calculations, and coercive field is related to the grain size and the domain wall velocity.[35,36] In addition, piezoelectric switching in γ-glycine has been observed[12] experimentally using a tip voltage of about 8 V, with an effective diameter of 8−10 nm, roughly corresponding to a maximum switching electric field of about 1 $V \cdot nm^{-1}$ at the

tip apex. Although it is not a direct experimental evidence, the similarity of the calculated and observed important field-strength magnitudes indicates that the calculated switching field is qualitatively realistic. This in turn supports the reliability of the large calculated value of the electric polarization in γ-glycine.

At the molecular level, Figure 3 depicts details of the spontaneous switching of a 10 × 10 × 10 supercell of γ-glycine

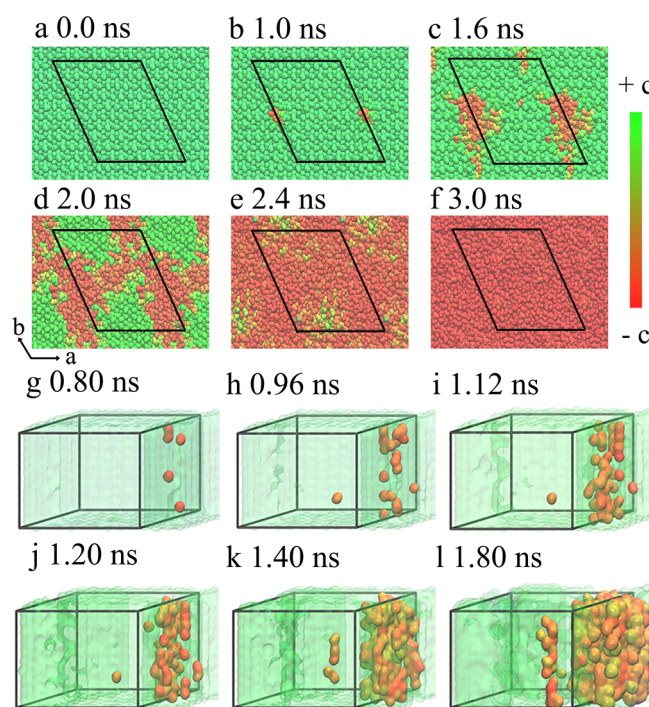**Figure 3.** Molecular dynamics simulations of polarization switching when γ-glycine at 300 K experiences an electric field of 1.5 V nm^{-1}. Molecules containing molecular dipoles with opposite orientations are displayed in green and red, respectively, for the domains having polarizations along the +c and −c directions. Panels a−f show alternatively oriented molecules shaded from red to green, revealing that the switching process is completed within approximately 1.5 ns. Panels g−l show details of the nucleating in three dimensions.

crystal from one ferroelectric orientation to the other, at 300 K and constant volume, under a driving electric field of 1.5 $V \cdot nm^{-1}$ applied for 5 ns. New domains begin to nucleate at about 1.0 ns, with ferroelectric switching complete after 3.0 ns. In this simulation, one single new domain initially appears at the left boundary of the cell, becoming a triangle-shaped domain after about 1.0 ns. This grows to fill the unit cell after 2.4 ns. From the three-dimensional plot of the nucleation process shown also in the figure, we find some locations in the system become reversed and then gradually connect into a cylindrical core. To validate our finding, we have repeated the MD simulation several times and obtained similar results for the ensemble of MD trajectories (see Figure S6).

Ferroelectric domain switching dynamics can be interpreted in terms of the Kolmogorov−Avrami−Ishibashi (KAI) model[37−40] based on classical statistical mechanics:

$$\Delta P(t) = 2P_s(1 - e^{-(t/t_0)^n}) \tag{1}$$

Here t_0 is the characteristic switching time, and P_s is the spontaneous polarization. We fit our MD results to this model to understand their domain kinetics. The fitted curve is shown
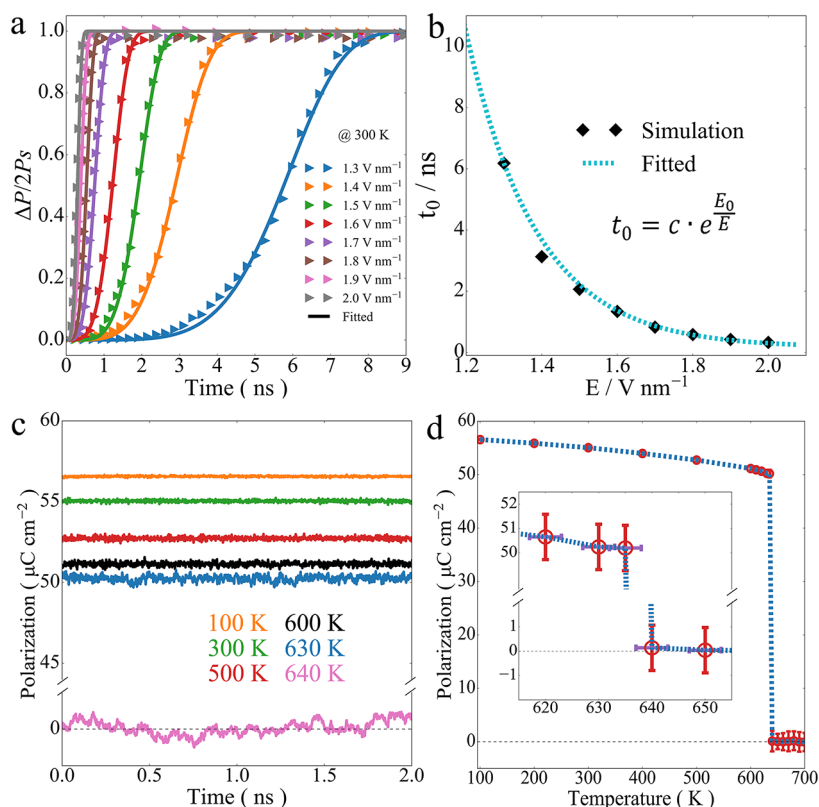
Figure 4. (a) Time-dependent evolution of the growing domain volume fraction during the switching process under different electric field strengths, with the solid lines corresponding to fitted results using the KAI model. (b) Activation electric field obtained with the characteristic switching time and the electric field, with the dotted line corresponding to the fitting result of the function. (c) Polarization profiles from MD simulations below and above the phase transition temperature for 2 ns. (d) Phase transition behavior of γ-glycine. The standard deviation of polarization is indicated by the vertical error bars at each point.

in Figure 4a,b, depicting the fractional conversion from one phase to the other at the different applied field strengths used. Different onset times associated with activated nucleation processes are revealed, followed by a growth stage that depends quite differently on the applied field, in accordance with model expectations. We also verified the convergence of the results with time to ensure accurate results using the ensemble of our MD trajectories mentioned above. The validation is shown in Table S2. The converged parameters t_0 and n are listed in Table 1.

To illustrate the relationship between t_0 and the strength of electric field E, we utilize Miller and Weinreich's relationship found previously in $BaTiO_3$:[39,41]

$$t_0 = c \cdot e^{E_0/E} \qquad (2)$$

Table 1. Electric Field Strength (E) and the Characteristic Switching Time (t_0)

E (V·nm^{-1})	t_0 (ns)	n
1.3	6.179	5.208
1.4	3.128	4.471
1.5	2.064	4.916
1.6	1.338	4.217
1.7	0.824	3.997
1.8	0.583	4.342
1.9	0.423	3.680
2.0	0.328	4.117

By least-squares fitting, the activation electric field of glycine is determined to be $E_0 = 11.05$ V·nm^{-1}, as shown in Figure 4b.

In different simulations, domain cores appeared at different locations, but the time-dependent evolutions of the growing domains during the switching processes are all similar. In more extensive simulations, the physical processes controlling these responses could be determined. Of particular importance would be how these responses change with external fields, such as temperature, pressure, doping, or chemical substitution, hence suggesting possible directions for future device research.

Because, in practical applications ferroelectricity would normally need to be maintained over some temperature range, we investigate the transition temperature of the ferroelectric phase of γ-glycine over the temperature range 100−700 K by MD. Results are shown in Figure 4c,d. As the temperature approaches 630 K, the average value of the polarization gradually decreases and its fluctuation increases. When the temperature reaches 640 ± 5 K, the polarization drops sharply to 0.0 μC·cm^{-2}, indicating that the ferroelectric phase transitions to a paraelectric one. The predicted sharp variation of the polarization is suggestive of a first-order phase transition, a result which is profoundly different from that found for the classical ferroelectric material triglycine sulfate (TGS), which instead displays a second-order phase transition.[42] The calculated order−disorder phase transition temperature of 630 ± 5 K for γ-glycine is much higher than the experimentally observed decomposition temperature of the material of about 500 K.[43] Hence, the simulations indicate that

glycine will display good ferroelectric properties, a requirement for device and biological applications.

In conclusion, we investigated the ferroelectric polarization of β-phase (monoclinic, $P2_1$) and two γ-phases (trigonal, $P3_1$ and $P3_2$) of glycine based on first-principles calculations and MPT. Our results predict that γ-glycine should have a spontaneous polarization of about 70.9 $\mu C \cdot cm^{-2}$ at 300 K. In addition, classical molecular dynamics simulations using PCC charges predict that the polarization of γ-glycine crystals will saturate completely at applied electric field strengths exceeding 1 $V \cdot nm^{-1}$. The ferroelectric–paraelectric phase transition is predicted to occur at 630 K, a value higher than the decomposition temperature of glycine. We also show that the switching process agrees with the KAI model, featuring separate time scales for nucleation of the product phase and its subsequent growth. Future studies need to explore the factors controlling each stage to determine how devices will respond to stimuli such as external temperature and pressure changes, doping, and chemical substitution. Given the critical role of glycine in biology, we hope the biocompatibility and ferroelectricity of glycine crystals will make them promising candidates for biomedical applications.

ASSOCIATED CONTENT

Ⓢ Supporting Information

The Supporting Information is available free of charge on the ACS Publications website at DOI: 10.1021/acs.jpclett.8b03837.

> Detailed crystal structures of the major phases of glycine crystal, benchmark results of different functionals, density of states of glycine, repeated simulation results, and simulation methods (PDF)

AUTHOR INFORMATION

Corresponding Authors
*E-mail: yongleli@t.shu.edu.cn.
*E-mail: alessandro.stroppa@spin.cnr.it.
*E-mail: renwei@shu.edu.cn.

ORCID
Shunbo Hu: 0000-0003-0472-0999
Jeffrey R. Reimers: 0000-0001-5157-7422
Andrew M. Rappe: 0000-0003-4620-6496
Yongle Li: 0000-0003-0515-6613
Wei Ren: 0000-0001-7317-3867

Notes
The authors declare no competing financial interest.

ACKNOWLEDGMENTS

REFERENCES

(1) Li, J.; Liu, Y.; Zhang, Y.; Cai, H. L.; Xiong, R. G. Molecular ferroelectrics: where electronics meet biology. *Phys. Chem. Chem. Phys.* **2013**, *15*, 20786–20796.

(2) Fukada, E. Piezoelectricity of Wood. *J. Phys. Soc. Jpn.* **1955**, *10*, 149–154.

(3) Liu, Y.; Zhang, Y.; Chow, M. J.; Chen, Q. N.; Li, J. Biological ferroelectricity uncovered in aortic walls by piezoresponse force microscopy. *Phys. Rev. Lett.* **2012**, *108*, 078103.

(4) Pal, M.; Guo, R.; Bhalla, A. Biological ferroelectricity in human nail samples using Piezoresponse Force Microscopy. *Mater. Res. Innovations* **2013**, *17*, 442–447.

(5) Cochran, G. V.; Pawluk, R. J.; Bassett, C. A. Stress generated electric potentials in the mandible and teeth. *Arch. Oral Biol.* **1967**, *12*, 917–920.

(6) Li, T.; Zeng, K. Nanoscale piezoelectric and ferroelectric behaviors of seashell by piezoresponse force microscopy. *J. Appl. Phys.* **2013**, *113*, 187202.

(7) Kholkin, A.; Amdursky, N.; Bdikin, I.; Gazit, E.; Rosenman, G. Strong piezoelectricity in bioinspired peptide nanotubes. *ACS Nano* **2010**, *4*, 610–614.

(8) Heredia, A.; Bdikin, I.; Kopyl, S.; Mishina, E.; Semin, S.; Sigov, A.; German, K.; Bystrov, V.; Gracio, J.; Kholkin, A. L. Temperature-driven phase transformation in self-assembled diphenylalanine peptide nanotubes. *J. Phys. D: Appl. Phys.* **2010**, *43*, 462001.

(9) Fukada, E.; Yasuda, I. On the Piezoelectric Effect of Bone. *J. Phys. Soc. Jpn.* **1957**, *12*, 1158–1162.

(10) Liu, Y.; Cai, H. L.; Zelisko, M.; Wang, Y.; Sun, J.; Yan, F.; Ma, F.; Wang, P.; Chen, Q. N.; Zheng, H.; et al. Ferroelectric switching of elastin. *Proc. Natl. Acad. Sci. U. S. A.* **2014**, *111*, E2780–E2786.

(11) Hu, S.; Jia, F.; Marinescu, C.; Cimpoesu, F.; Qi, Y.; Tao, Y.; Stroppa, A.; Ren, W. Ferroelectric polarization of hydroxyapatite from density functional theory. *RSC Adv.* **2017**, *7*, 21375–21379.

(12) Heredia, A.; Meunier, V.; Bdikin, I. K.; Gracio, J.; Balke, N.; Jesse, S.; Tselev, A.; Agarwal, P. K.; Sumpter, B. G.; Kalinin, S. V.; et al. Nanoscale Ferroelectricity in Crystalline γ-Glycine. *Adv. Funct. Mater.* **2012**, *22*, 2996–3003.

(13) Guerin, S.; Stapleton, A.; Chovan, D.; Mouras, R.; Gleeson, M.; McKeown, C.; Noor, M. R.; Silien, C.; Rhen, F. M. F.; Kholkin, A. L.; et al. Control of piezoelectricity in amino acids by supramolecular packing. *Nat. Mater.* **2017**, *17*, 180–186.

(14) Elsila, J. E.; Dworkin, J. P.; Bernstein, M. P.; Martin, M. P.; Sandford, S. A. Mechanisms of Amino Acid Formation in Interstellar Ice Analogs. *Astrophys. J.* **2007**, *660*, 911–918.

(15) Boldyreva, E. V.; Drebushchak, T. N.; Shutova, E. S. Structural distortion of the α, β, and γ polymorphs of glycine on cooling. *Z. Kristallogr. - Cryst. Mater.* **2003**, *218*, 366–376.

(16) Albrecht, G.; Corey, R. B. The Crystal Structure of Glycine. *J. Am. Chem. Soc.* **1939**, *61*, 1087–1103.

(17) Dawson, A.; Allan, D. R.; Belmonte, S. A.; Clark, S. J.; David, W. I. F.; McGregor, P. A.; Parsons, S.; Pulham, C. R.; Sawyer, L. Effect of High Pressure on the Crystal Structures of Polymorphs of Glycine. *Cryst. Growth Des.* **2005**, *5*, 1415–1427.

(18) Goryainov, S. V.; Boldyreva, E. V.; Kolesnik, E. N. Raman observation of a new (ζ) polymorph of glycine? *Chem. Phys. Lett.* **2006**, *419*, 496–500.

(19) Iitaka, Y. Crystal Structure of β-Glycine. *Nature* **1959**, *183*, 390–391.

(20) Iitaka, Y. The crystal structure of γ-glycine. *Acta Crystallogr.* **1961**, *14*, 1–10.

(21) Perlovich, G. L.; Hansen, L. K.; Bauer-Brandl, A. The Polymorphism of Glycine. Thermochemical and structural aspects. *J. Therm. Anal. Calorim.* **2001**, *66*, 699−715.

(22) Park, K.; Evans, J. M. B.; Myerson, A. S. Determination of Solubility of Polymorphs Using Differential Scanning Calorimetry. *Cryst. Growth Des.* **2003**, *3*, 991−995.

(23) Bystrov, V. S.; Seyedhosseini, E.; Bdikin, I.; Kopyl, S.; Neumayer, S. M.; Coutinho, J.; Kholkin, A. L. Bioferroelectricity in Nanostructured Glycine and Thymine: Molecular Modeling and Ferroelectric Properties at the Nanoscale. *Ferroelectrics* **2015**, *475*, 107−126.

(24) Resta, R.; Vanderbilt, D. Theory of Polarization: A Modern Approach. *Topics Appl. Phys.* **2007**, *105*, 31−68.

(25) Stroppa, A.; Quarti, C.; De Angelis, F.; Picozzi, S. Ferroelectric Polarization of $CH_3NH_3PbI_3$: A Detailed Study Based on Density Functional Theory and Symmetry Mode Analysis. *J. Phys. Chem. Lett.* **2015**, *6*, 2223−2231.

(26) Hu, S.; Gao, H.; Qi, Y.; Tao, Y.; Li, Y.; Reimers, J. R.; Bokdam, M.; Franchini, C.; Di Sante, D.; Stroppa, A.; Ren, W. Dipole Order in Halide Perovskites: Polarization and Rashba Band Splittings. *J. Phys. Chem. C* **2017**, *121*, 23045−23054.

(27) Perdew, J. P.; Burke, K.; Ernzerhof, M. Generalized Gradient Approximation Made Simple. *Phys. Rev. Lett.* **1996**, *77*, 3865−3868.

(28) Stroppa, A.; Di Sante, D.; Barone, P.; Bokdam, M.; Kresse, G.; Franchini, C.; Whangbo, M. H.; Picozzi, S. Tunable ferroelectric polarization and its interplay with spin-orbit coupling in tin iodide perovskites. *Nat. Commun.* **2014**, *5*, 5900.

(29) Ye, H.-Y.; Tang, Y.-Y.; Li, P.-F.; Liao, W.-Q.; Gao, J.-X.; Hua, X.-N.; Cai, H.; Shi, P.-P.; You, Y.-M.; Xiong, R.-G. Metal-free three-dimensional perovskite ferroelectrics. *Science* **2018**, *361*, 151−155.

(30) Li, P.-F.; Tang, Y.-Y.; Liao, W.-Q.; Shi, P.-P.; Hua, X.-N.; Zhang, Y.; Wei, Z.; Cai, H.; Xiong, R.-G. Experimental Evidence for a Triboluminescent Antiperovskite Ferroelectric: Tris-(trimethylammonium) catena-Tri-μ-chloro-manganate(II) Tetrachloromanganate(II). *Angew. Chem., Int. Ed.* **2018**, *57*, 11939−11942.

(31) Li, P.-F.; Liao, W.-Q.; Tang, Y.-Y.; Ye, H.-Y.; Zhang, Y.; Xiong, R.-G. Unprecedented Ferroelectric−Antiferroelectric−Paraelectric Phase Transitions Discovered in an Organic−Inorganic Hybrid Perovskite. *J. Am. Chem. Soc.* **2017**, *139*, 8752−8757.

(32) Li, Y. L.; Mei, Y.; Zhang, D. W.; Xie, D. Q.; Zhang, J. Z. H. Structure and Dynamics of a Dizinc Metalloprotein: Effect of Charge Transfer and Polarization. *J. Phys. Chem. B* **2011**, *115*, 10154−10162.

(33) Tong, Y.; Mei, Y.; Li, Y. L.; Ji, C. G.; Zhang, J. Z. H. Electrostatic Polarization Makes a Substantial Contribution to the Free Energy of Avidin−Biotin Binding. *J. Am. Chem. Soc.* **2010**, *132*, 5137−5142.

(34) Jiang, A.-Q.; Lee, H. J.; Hwang, C. S.; Tang, T.-A. Resolving the Landauer paradox in ferroelectric switching by high-field charge injection. *Phys. Rev. B: Condens. Matter Mater. Phys.* **2009**, *80*, 024119.

(35) Shin, Y.-H.; Grinberg, I.; Chen, I.-W.; Rappe, A. M. Nucleation and growth mechanism of ferroelectric domain-wall motion. *Nature* **2007**, *449*, 881−884.

(36) Liu, S.; Grinberg, I.; Rappe, A. M. Intrinsic ferroelectric switching from first principles. *Nature* **2016**, *534*, 360−363.

(37) Jo, J. Y.; Han, H. S.; Yoon, J. G.; Song, T. K.; Kim, S. H.; Noh, T. W. Domain Switching Kinetics in Disordered Ferroelectric Thin Films. *Phys. Rev. Lett.* **2007**, *99*, 267602.

(38) Boddu, V.; Endres, F.; Steinmann, P. Molecular dynamics study of ferroelectric domain nucleation and domain switching dynamics. *Sci. Rep.* **2017**, *7*, 806.

(39) Shin, Y. H.; Grinberg, I.; Chen, I. W.; Rappe, A. M. Nucleation and growth mechanism of ferroelectric domain-wall motion. *Nature* **2007**, *449*, 881−884.

(40) Vopsaroiu, M.; Blackburn, J.; Cain, M. G.; Weaver, P. M. Thermally activated switching kinetics in second-order phase transition ferroelectrics. *Phys. Rev. B: Condens. Matter Mater. Phys.* **2010**, *82*, 024109.

(41) Miller, R. C.; Weinreich, G. Mechanism for the Sidewise Motion of 180° Domain Walls in Barium Titanate. *Phys. Rev.* **1960**, *117*, 1460−1466.

(42) Matthias, B. T.; Miller, C. E.; Remeika, J. P. Ferroelectricity of Glycine Sulfate. *Phys. Rev.* **1956**, *104*, 849−850.

(43) Weiss, I. M.; Muth, C.; Drumm, R.; Kirchner, H. Thermal decomposition of the amino acids glycine, cysteine, aspartic acid, asparagine, glutamic acid, glutamine, arginine and histidine. *BMC Biophys.* **2018**, *11*, 2.